Macromolecular Rapid Communications
www.mrc-journal.de

Design, Synthesis, and Theoretical Studies on the Benzoxadiazole and Thienopyrrole Containing Conjugated Random Copolymers for Organic Solar Cell Applications

Oguzhan Karakurt, Pelin Oral, Serife Ozdemir Hacioglu, Eda Alemdar Yılmaz, Tuğba Haciefendioğlu, Umran Isil Bicer, Egemen Ozcelik, Gonul Hizalan Ozsoy, Erol Yildirim, Levent Kamil Toppare, and Ali Cirpan**

In this study, six different donor-π-acceptor$_1$-π-donor-acceptor$_2$ type random co-polymers containing benzodithiophene as a donor, benzooxadiazole (BO), and thieno[3,4-c]pyrrole-4,6-dione (TPD) as acceptor, have been synthesized and characterized. In addition to the acceptor core ratio at different values, the effect of aromatic bridge structures on the optical, electronic, and photovoltaic properties of six different random co-polymers is investigated by using thiophene and selenophene structures as aromatic bridge units. To investigate how the acceptor unit ratio and replacement of aromatic bridge units impact the structural, electronic, and optical properties of the polymers, density functional theory (DFT) calculations are carried out for the tetramer models. The open-circuit voltage (V_{OC}), which is strongly correlated with the HOMO levels of the donor material, is enhanced with the increasing ratio of the TPD moiety. On the other hand, the short-circuit current (J_{SC}), which is associated with the absorption ability of the donor material, is improved by the increasing ratio of BO moiety with the π-bridges. BO moiety dominant selenophene π-bridged co-polymer (P_4) showed the best performance with a power conversion efficiency (PCE) of 6.26%, a J_{SC} of 11.44 mA cm^2, a V_{OC} of 0.80 V, and a fill factor (FF) of 68.81%.

1. Introduction

The world's energy needs are growing steadily, driven by population growth, rising demand, and consumption. As a result, traditional energy sources such as oil, coal, and natural gas are rapidly depleting. Researchers are exploring alternative, eco-friendly energy sources to address this challenge and meet our growing needs. Among the most promising options are solar cells, which can directly convert sunlight's abundant and renewable energy into electrical power. Conjugated polymers (CP) provide many advantages in organic photovoltaic technology, such as their lower production cost, lightweight, and flexibility. Thus, organic solar cells (OSCs) come to the forefront among other counterparts by enabling roll-to-roll production, output elasticity, and environmentally friendly production and annihilation methods.[1,2] Donor–acceptor copolymerization is the widely used method for improving conjugated polymer systems. The backbone of the conjugated polymer is characterized by a repeating pattern of alternating electron-rich and electron-deficient units along the polymer's backbone.[3,4] D–A conjugated polymers offer the following advantages: a) showing a broad absorption spectrum with high extinction coefficients to collect solar photons, b) showing favorable and tunable molecular energy levels that obtain matching with acceptors, c) showing

O. Karakurt, T. Haciefendioğlu, U. I. Bicer, E. Ozcelik, E. Yildirim, L. K. Toppare, A. Cirpan
Department of Chemistry
Middle East Technical University
Ankara 06800, Turkey
E-mail: toppare@metu.edu.tr; acirpan@metu.edu.tr

The ORCID identification number(s) for the author(s) of this article can be found under https://doi.org/10.1002/marc.202400343

DOI: 10.1002/marc.202400343

P. Oral, E. Yildirim, A. Cirpan
Department of Polymer Science and Technology
Middle East Technical University
Ankara 06800, Turkey

S. O. Hacioglu
Department of Basic Sciences of Engineering
Faculty of Engineering and Natural Sciences
Iskenderun Technical University
Hatay 31200, Turkey

E. A. Yılmaz
National Institute of Materials Physics
Laboratory of Functional Nanostructures
Atomistilor 405A, Magurele 077125, Romania

G. H. Ozsoy, A. Cirpan
ODTU GUNAM
Middle East Technical University
Ankara 06800, Turkey

improved charge mobility, which helps with charge separation and transport processes.[4,5]

Many different structures are used in the CP backbone, such as benzo[*c*] [1,2,5]triazole,[6–11] Benzo[*c*][1,2,5]thiadiazole,[12–18] Benzo[*c*][1,2,5]selenadiazole,[19–24] quinoxaline,[25–30] isoindigo,[31–35] Benzodithiophene,[36–41] thieno[3,4-c]pyrrole-4,6-dione,[42–48] pyrollo[3,4-c]pyrrole-1,4-dione.[12,49–53] Among these structures, benzodithiophene (BDT) has attracted significant interest as a donor moiety in D–A copolymers because of its molecular planarity and electron-rich nature. Using a BDT unit has additional benefits since its electrical and steric nature may be readily adjusted by an ordinary chemical change. High-performance OSCs have been achieved using an electron-rich BDT unit as a donor moiety.[54,55] Some substantial properties of the BDT structure are given below: a) The planarity of the two thiophene units is preserved while substituents can be incorporated into the central benzene core thanks to the fused BDT ring structure; b) The structural symmetry and rigid fused aromatic system of the polymer can improve charge mobility and eliminate the requirement to control regioregularity during polymerization. Additionally, this will help to enhance electron delocalization and interchain interactions,[56] and c) These properties will allow the low HOMO energy level of the resulting polymers to be maintained, as demonstrated by donor-strong and acceptor-weak polymers.[56–59] Benzo[*c*][1,2,5]oxadiazole (BO) is a potent electron-withdrawing moiety commonly utilized in OSCs due to its planar, rigid geometry, ease of synthesis, good stability, and optoelectronic properties. BO-based polymers have low-bandgaps and coplanar structures owing to their capability to adopt the quinoid structure in the polymer. The excellent solubility of conductive polymers is critical for high-quality film formation and purification in optoelectronic devices. While the polymer chain may have a planar conformation, the 5,6-bis alkoxyl substitution of BO is highly beneficial for creating conjugated polymers with improved solubility and higher molecular weight.[60,61] Thieno[3,4-c]pyrrole-4,6-dione (TPD) has widely been used to prepare both acceptor and donor materials for OSCs. It has become an essential component for polymer backbone due to its strong electron-accepting ability, symmetrical geometry, rigidity, and structural properties. Due to these properties, it regulates the HOMO – LUMO energy levels. Attributed to its diimide structure, it keeps the LUMO level constant while lowering HOMO levels, which is crucial for increasing the open-circuit voltage (V_{OC}).[54,62,63]

Bridging aromatic units plays a critical role in the electronic structure of the backbone polymer and the interaction between the donor and acceptor units. As a result, they significantly impact the structure and, consequently, the optical, electrochemical, charge transport, and photovoltaic properties of D-π-A conjugated copolymers. Therefore, to design novel polymers for efficient OPVs, it is crucial to fully understand how the π-bridges affect the physicochemical and photovoltaic properties.[64] In the literature, thiophene is a widely used bridging aromatic unit. Modifications on these aromatic units are frequently applied in the literature to investigate the effect of bridging aromatic units on the optical, electronic, and photovoltaic properties of CPs. A way to achieve this is by replacing the sulfur (S) atoms in the thiophene aromatic rings with selenium (Se) atoms. Selenophene is a homolog of chalcogenophene that shares chemical and physical similarities with thiophene. Its relatively lower aromaticity enhances the ground-state quinoid resonance character of the resulting polymers, leading to improved planarity, increased effective conjugation length, and lower band-gap energy. The selenium (Se) atom exhibits a larger atomic radius and lower electronegativity than the sulfur (S) atom. Consequently, polymers incorporating Se display a greater capacity for broadening the absorption spectrum, particularly in the infrared region. Furthermore, the Se-containing constituents are characterized by higher polarizability in contrast to their sulfur-containing analogs, resulting in improved charge mobility within the polymer, primarily attributed to the Se···Se interactions that occur between polymer chains.[65–68]

In this study, six different new donor-π-acceptor$_1$-π-donor-acceptor$_2$ type random co-polymer structures were prepared by using thiophene and selenophene bridges in polymer structures containing BDT as donor and BO and TPD as acceptors. The impact of the π-bridge and acceptor core ratios was thoroughly studied in terms of optical, electrochemical, and photovoltaic functionality in these designs. The properties of **P1-P3** and **P4-P6** changed as the π-bridge was chosen as thiophene and selenophene, respectively. The bandgaps of the **P1** and **P4** were tuned from 1.70 to 1.67 eV, with HOMO levels decreasing from -5.52 to -5.61 eV. The maximum absorption wavelengths λ_{max} were shifted from 587/633 nm to 606/650 nm, respectively. This study presents the highest PCE value of **6.29%** with a short-circuit density (J_{SC}) of 11.44 mA cm^{-2}, an open-circuit voltage (V_{OC}) of 0.80 V, and a fill factor (FF) of 68.81%, which was achieved with applying a modification on polymer backbone by incorporating a selenophene bridge and TPD moiety.

2. Result and Discussion

2.1. Synthesis of Characterization

The TPD acceptor unit and BDT donor unit were commercially supplied. The synthetic pathway of oxadiazole-based acceptor cores is presented in **Scheme 1**. All the intermediary products and monomers were synthesized according to adopted procedures from the literature. Detailed synthetic information on obtaining oxadiazole-based monomers (**M1** and **M2**) is provided in the supporting information. In general, to obtain compound **1** (1,2-bis(octyloxy)benzene), Williamson ether synthesis was performed, and the target molecule was obtained with a high yield. After that, a nitration reaction in the presence of fuming nitric acid (100% HNO_3) and acetic acid was performed, and compound **2** (1,2-dinitro-4,5-bis(octyloxy)benzene) was obtained with a high yield. To achieve the oxadiazole main core, a ring-closure reaction with tri-phenyl phosphine (PPh_3) and sodium azide (NaN_3) is performed, and target molecule **3** (5,6-bis (octyloxy)benzo [c][1,2,5]oxadiazole) was achieved with a moderate yield. To obtain molecule **4** (4,7-dibromo-5,6-bis(octyloxy)benzo[c][1,2,5]oxadiazole), a bromination reaction was conducted with molecular bromine (Br_2) and acetic acid. Stanylated compounds **5** (tributyl(thiophen-2-yl) stannane) and **6** (tributyl(selenophen-2-yl)stannane) were prepared using n-butyl lithium (*n*-BuLi) and tributyltin chloride ($SnBu_3Cl$). After achieving molecule **4** with a good yield, the Stille Cross-Coupling was applied in the presence of a palladium catalyst, and the carbon-

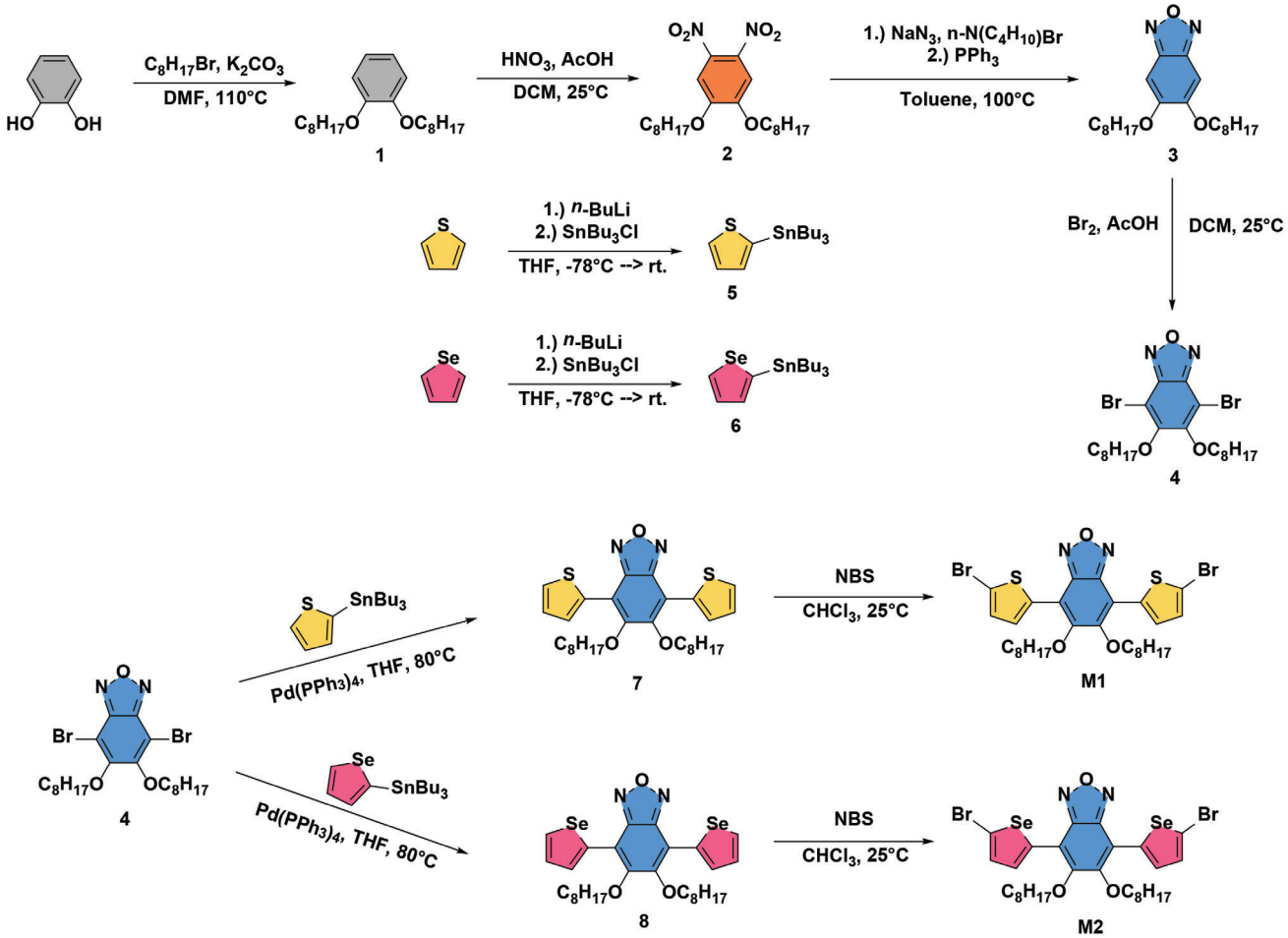

Scheme 1. Synthetic Pathway of M1 and M2.

carbon bond was constituted between molecule **4** and stanylated compounds, and molecules **7** (5,6-bis(octyloxy)-4,7-di(thiophen-2-yl)benzo[c][1,2,5]oxadiazole) and **8** (5,6-bis(octyloxy)-4,7-di(selenophen-2-yl)benzo[c][1,2,5]oxadiazole) were obtained with a good yield. Finally, a bromination reaction by using *n*-bromo succinimide was performed, and target monomers **M1** (4,7-bis(5-bromothiophen-2-yl)-5,6-bis(octyloxy) benzo [c] [1,2,5] oxadiazole) and **M2** (4,7-bis(5-bromoselenophen-2-yl)-5,6-bis (octyloxy) benzo [c] [1,2,5] oxadiazole) were obtained with a high yield.[5,60,61] All the intermediary products and monomers were characterized by ^{1}H and ^{13}C NMR (nuclear magnetic resonance).

Stille polycondensation reactions were performed via Palladium catalysts to synthesize target polymers (**P1**, **P2**, **P3**, **P4**, **P5**, **P6**). While **D1** was used as a donor unit, **M1**, **M2**, and **M3** were used as acceptor monomers. Polymerization reactions were conducted under a nitrogen atmosphere, and chlorobenzene was used as the reaction solvent.[69,70] To determine the molecular weights and polydispersity index (PDI) values of the polymers, GPC (gel permeation chromatography) was used. For the structural analysis, IR spectroscopy was used, and functional groups of the polymers were verified. Finally, TGA (thermal gravimetric analysis) was conducted to examine the polymers' thermal behaviors and decomposition temperatures. In **Scheme 2**. Synthetic pathways of the polymers were illustrated. The reaction conditions and summary of the characterization data are summarized in **Table 1**. Further synthetic details and spectra are given in supporting information.

2.2. Thermal Studies

To analyze the thermal stability of the polymers, thermogravimetric analysis (TGA) measurements were performed. All the polymers showed satisfying thermal stability with decomposition temperatures above 300 °C, which refers to the first sharp weight (5.0%) loss. The increasing trend of decomposition temperatures from **P1** to **P3** and **P4** to **P6** can be explained by the rising ratio of TPD units in the polymer backbone since the BO unit with π-bridge is larger and more complex than the TPD core. These decomposition temperatures are adequate for photovoltaic applications in Table 1. results of TGA analysis are summarized, and thermograms of the polymers are provided in supporting information.

2.3. Electrochemical Studies

Cyclic voltammetry (CV) is a functional and widely preferred technique to investigate the doping behaviors, HOMO–LUMO

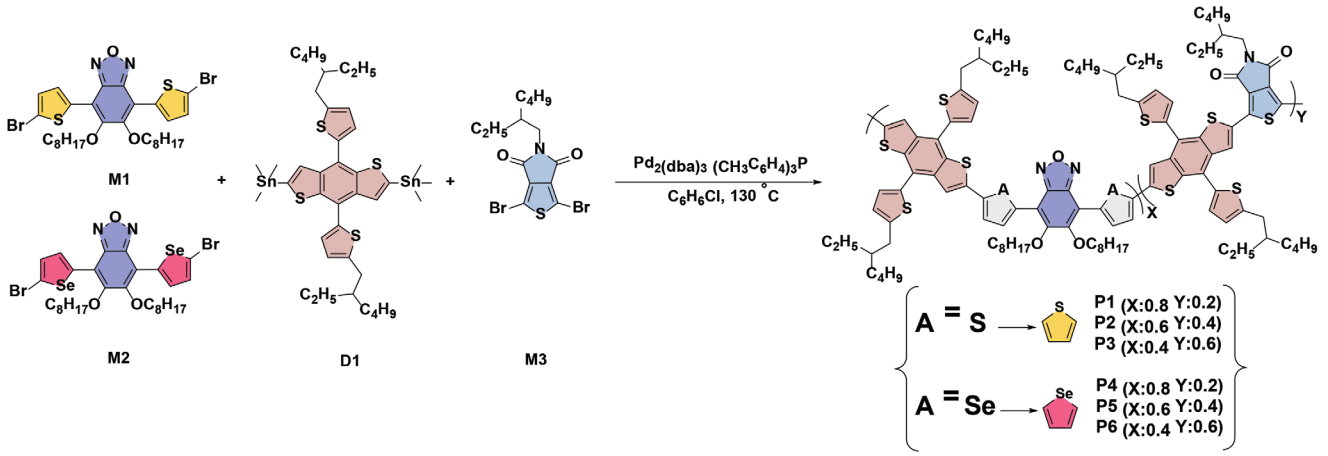

Scheme 2. Synthetic pathways of the target polymer.

energy levels, and electronic bandgaps of the polymers. Herein, redox features of obtained polymers were examined with CV in 0.1 M tetrabutylammonium hexafluorophosphate/acetonitrile ($TBAPF_6$/ACN) electrolyte/solvent couple. Before electrochemical characterizations, chemically obtained polymers were dissolved in chloroform solution (5 mg mL^{-1}) and spray coated on the ITO working electrodes, and studies were performed with a 100 mV s^{-1} scan rate. Single-scan CVs of six polymers were reported in **Figure 1**. All polymers exhibited p-type and n-type doping characters, which means the polymers have an ambipolar character. Doping potentials of **P1**, **P2**, and **P3** during p-type doping are 1.15, 1.32, and 1.55 V. Furthermore, **P1**, **P2**, and **P3** have a reversible redox couple during n-type doping centered at −1.22, −1.27, and −1.26 V. Doping and dedoping potentials of **P4**, **P5**, **P6** during p-type doping are 1.21, 1.30, and 1.35 V. Additionally, **P4**, **P5**, **P6** have a reversible redox couple during n-type doping centered at −1.17, −1.51, and −1.31 V.

Another important parameters for electrochemical characterizations are HOMO/LUMO energy levels, which can be calculated from CVs. HOMO/LUMO energy levels were calculated from the onset of the oxidation of the p-doping state and the onset of the reduction of the n-doping state by using Equation (1) and Equation (2), respectively. The corresponding HOMO/LUMO energy levels were calculated and reported as −5.52 and −3.81 eV for **P1**, −5.74 and −3.71 eV for **P2**, −5.86 and −3.78 eV for **P3**, −5.61 and −3.77 eV for **P4**, −5.67 and −3.67 eV for **P5** and −5.80 and −3.65 eV for **P6** (**Table 2**).

$$\text{HOMO} = -\left(E_{ox,\,onset} + 4.75\right)\ \text{eV} \quad (1)$$

$$\text{LUMO} = -\left(E_{red,\,onset} + 4.75\right)\ \text{eV} \quad (2)$$

In **Figure 2**, the energy level diagram is illustrated, which is evidential reasoning the HOMO & LUMO levels of the polymers

Table 1. GPC and TGA results of terpolymers.

Polymers	Equivalency			Temperature & Time [a]	Yield	GPC	T_d [b]
P1	**D1**	**M1**	**M3**	130 °C	83%	Mn = 47 kDa	312 °C
	1.0	0.8	0.2	26 h		Mw = 77 kDa	
						PDI = 1.64	
P2	**D1**	**M1**	**M3**	130 °C	76%	Mn = 46 kDa	328 °C
	1.0	0.6	0.4	30 h		Mw = 94 kDa	
						PDI = 2.04	
P3	**D1**	**M1**	**M3**	130 °C	81%	Mn = 44 kDa	348 °C
	1.0	0.4	0.6	29 h		Mw = 85 kDa	
						PDI = 1.93	
P4	**D1**	**M2**	**M3**	130 °C	77%	Mn = 116 kDa	306 °C
	1.0	0.8	0.2	22 h		Mw = 195 kDa	
						PDI = 1.68	
P5	**D1**	**M2**	**M3**	130 °C	76%	Mn = 98.8 kDa	320 °C
	1.0	0.6	0.4	24 h		Mw = 206 kDa	
						PDI = 2.09	
P6	**D1**	**M2**	**M3**	130 °C	83%	Mn = 80.1 kDa	325 °C
	1.0	0.4	0.6	24 h		Mw = 120.3 kDa	
						PDI = 1.50	

[a] 8 mL chlorobenzene was used as a reaction solvent for all polymerizations; [b] Refers to 5% weight loss in TGA analysis.

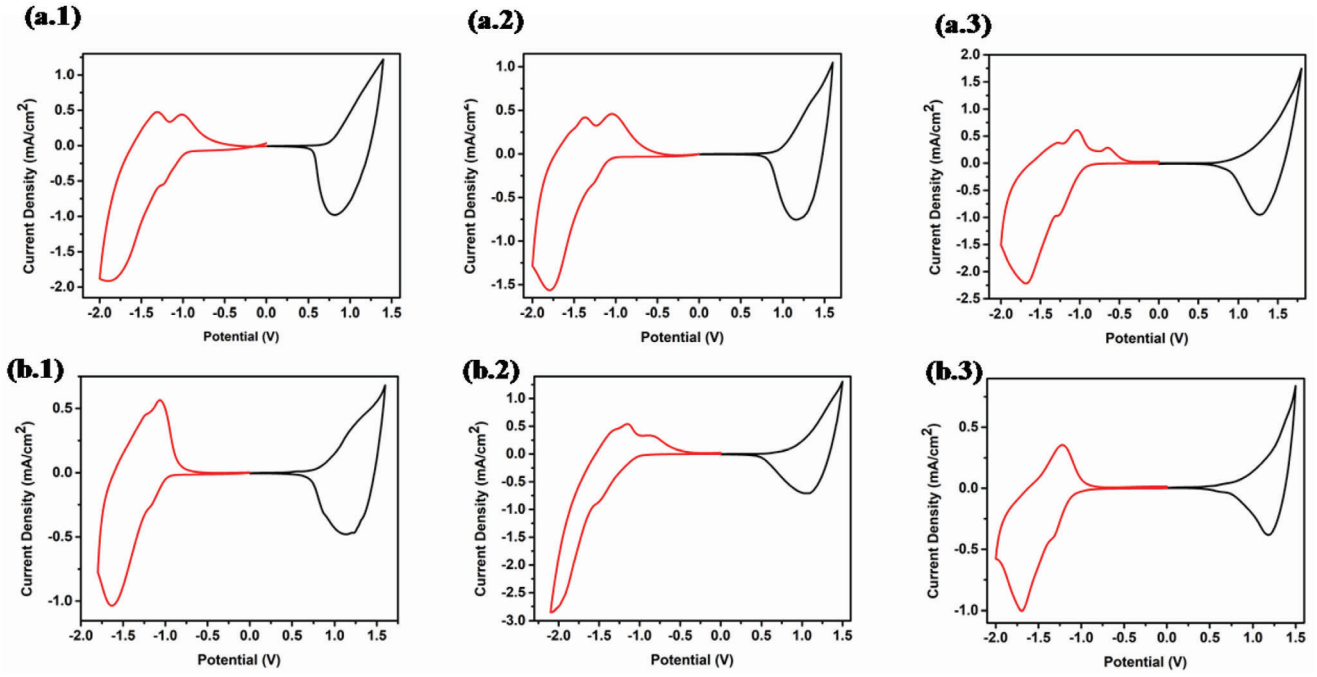

Figure 1. Single scan cyclic voltammograms of a.1) **P1**, a.2) **P2**, a.3) **P3**, b.1) **P4**, b.2) **P5** and b.3) **P6** in 0.1 M $TBAPF_6$/ACN solution.

are suitable to create the charge transfer between the polymers, PEDOT: PSS, and $PC_{71}BM$. All electrochemical characterizations for six polymers were demonstrated in Table 2. When **P1**, **P2**, and **P3** were compared in terms of electrochemical properties, the oxidation potentials were increased from **P1** (1.15 V) to **P3** (1.55 V) as the ratio of benzoxadiazole unit decreasing in the copolymer structure, which can be dedicated to the higher electron density of benzoxadiazole unit compared with DPP unit. Regarding electrochemical properties, a similar trend can be seen for **P4**, **P5**, and **P6**. As seen in Table 2, the oxidation potentials were increased from **P4** (1.21 V) to **P6** (1.35 V) as the ratio of benzoxadiazole unit decreased in the copolymer structure, which can be explained by the higher electron density of benzoxadiazole unit with the π-bridges.

2.4. Optical Studies

Spectroelectrochemical studies were performed by recording the changes in the absorption spectra via stepwise oxidation by UV–vis-NIR spectrophotometer to investigate the optical properties, formation of charge carriers, and calculate optical bandgap. For spectroelectrochemical studies, all polymers (**P1**, **P2**, **P3**, **P4**, **P5**, and **P6**) were dissolved in $CHCl_3$ and spray-coated onto ITO electrodes, similar to the electrochemical studies. The potentials were swept from 0.0 to 1.4 V for **P1**, from 0.0 to 1.4 V for **P2**, from 0.0 to 1.5 V for **P3**, from 0.0 to 1.4 V for **P4**, from 0.0 to 1.3 V for **P5** and from 0.0 to 1.45 V for **P6** in 0.1 M ACN/$TBAPF_6$ solution. During stepwise oxidation, the absorption of the π–π^* transition decreased; moreover, new absorption bands started to appear at ≈800 nm and 1600–1800 nm for all polymers (**P1**, **P2**, **P3**, **P4**, **P5**, and **P6**) which could be dedicated to the formation of free charge carriers such as polarons (radical cations) and bipolarons (dications). Electronic absorption spectra of the polymers were provided in supporting information. Spectroelectrochemical characterizations are important for conducting polymers, especially determining crucial parameters such as λ_{max} and optical bandgap (E_g^{op}) values. The λ_{max} values were recorded as 587/633 nm for **P1**, 589/619 nm for **P2**, 569/609 nm for **P3**, 606/650 nm for **P4**, 606/654 nm for **P5** and 560/608 nm for **P6** (**Figure 3**).

Table 2. Summary of electrochemical and optical properties of the polymers.

Polymers	$E_{p\text{-doping}}$ (V)	$E_{p\text{-onset}}$ (V)	$E_{n\text{-doping}}$ (V)	$E_{n\text{-onset}}$ (V)	HOMO (eV)	LUMO (eV)	E_g^{ec} [a] (eV)	λ_{max} (nm)	λ_{max}^{onset} (nm)	E_g^{op} [b] (eV)
P1	1.15	0.77	−1.22	−0.94	−5.52	−3.81	1.71	587/633	726	1.70
P2	1.32	0.99	−1.27	−1.04	−5.74	−3.71	2.03	589/619	737	1.70
P3	1.55	1.11	−1.26	−0.97	−5.86	−3.78	2.08	569/609	705	1.76
P4	1.21	0.86	−1.17	−0.98	−5.61	−3.77	1.84	606/650	739	1.67
P5	1.30	0.92	−1.51	−1.08	−5.67	−3.67	2.00	606/654	738	1.68
P6	1.35	1.05	−1.31	−1.10	−5.80	−3.65	2.15	560/608	720	1.72

[a] Electronical bandgap; [b] Optical bandgap.

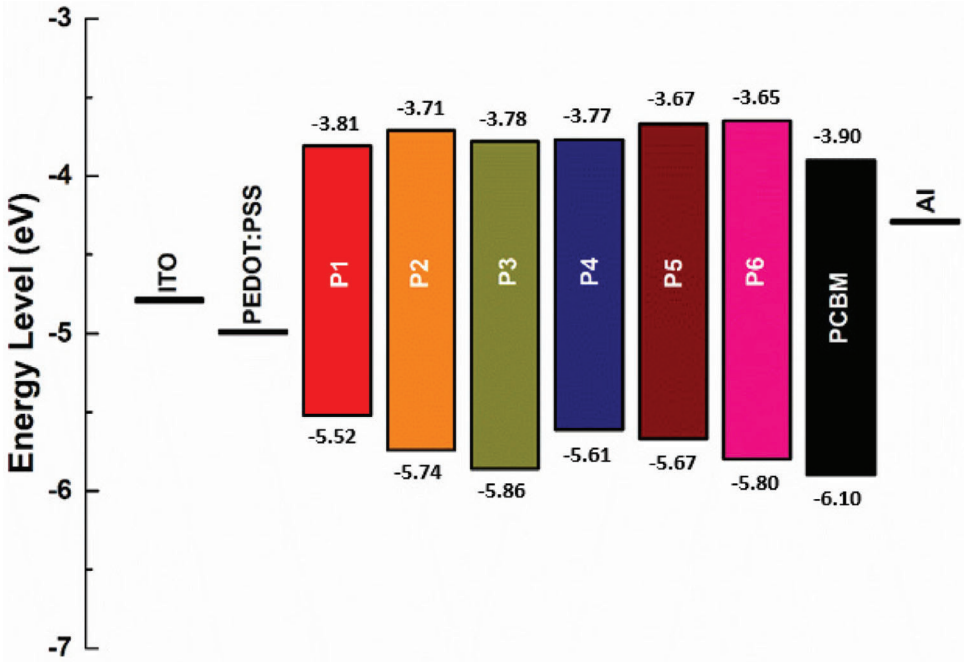

Figure 2. Representation of combined energy level diagram of solar devices.

As usual, optical bandgaps were calculated from the onsets of lowest energy π–π^* transitions as 1.70 eV (**P1**), 1.68 eV (P2), 1.76 eV (P3), 1.67 eV (P4), 1.68 eV (P5) and 1.72 eV (P6) (Table 2). The results of spectroelectrochemical characterizations for six polymers are demonstrated in Table 2. From Table 2, the effect of selenophene can be noticed. Polymers with selenophene have broader and red-shifted absorption spectra in both thin-film and solution states. Another point is that polymers with a dominant ratio of BO unit have better absorption ability, which could be attributed to the higher electron density of BO unit with the π-bridges. All the polymers showed red-shift action from solution to thin-film state, which can be explained by aggregation of

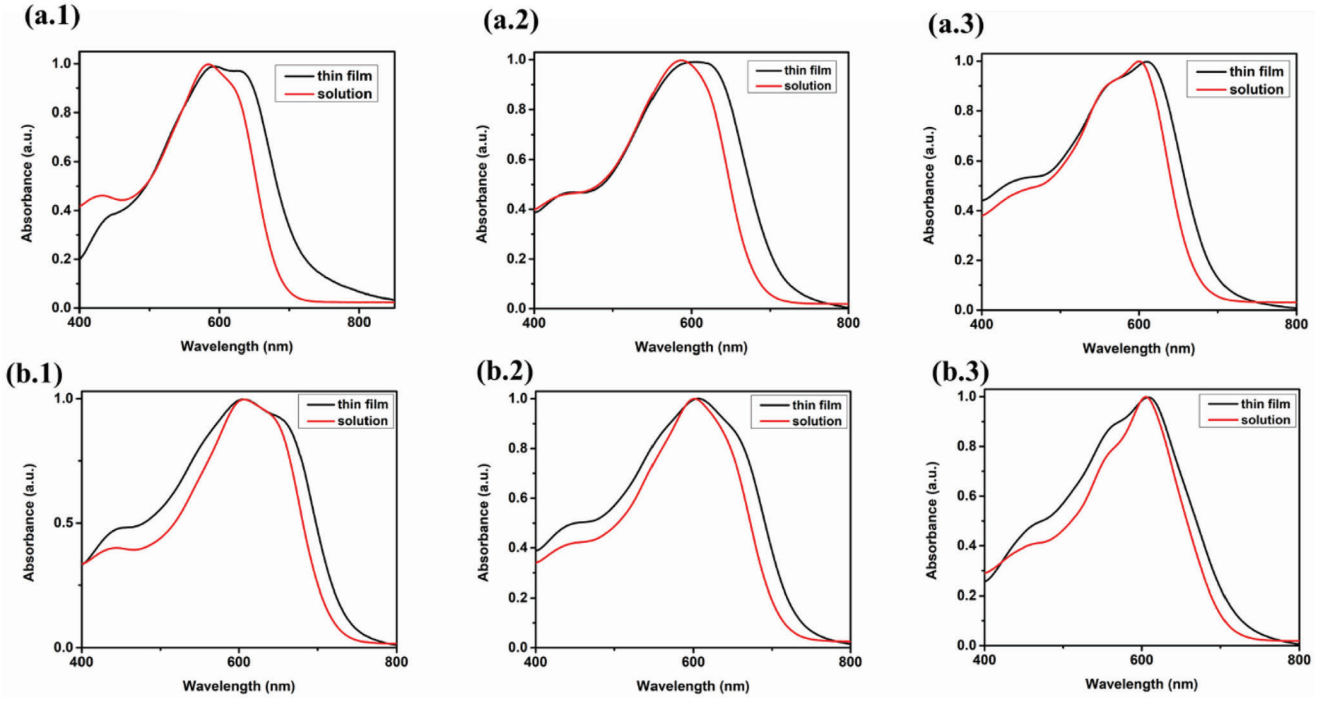

Figure 3. Normalized absorption spectra of both solution and thin-film states of a.1) **P1**, a.2) **P2**, a.3) **P3**, b.1) **P4**, b.2) **P5** and b.3) **P6**.

Table 3. Electronic and structural properties based on the DFT calculations.

	E_g (eV)	HOMO (eV)	LUMO (eV)	λ_{max} (nm)	VIP (eV)	AIP (eV)	λ_{reorg} (eV)	E_g^{op} (eV)	μ (Debye)	α (a.u.)	β (a.u.)	γ (a.u.)
P1$_t$	1.94	−5.07	−3.13	641	−5.57	−5.51	0.0038	1.49	2.36	3652.03	5147.81	34201.56
P2$_t$	1.97	−5.09	−3.12	640	−5.64	−5.58	0.0042	1.51	2.59	3325.94	4420.01	88746.41
P3$_t$	2.10	−5.16	−3.07	607	−5.74	−5.69	0.0041	1.60	2.76	2946.77	3642.94	78805.77
P4$_t$	1.95	−5.00	−3.06	726	−5.54	−5.48	0.0037	1.68	2.59	3878.52	5764.67	38443.38
P5$_t$	2.01	−5.05	−3.04	710	−5.61	−5.55	0.0044	1.71	2.79	3487.87	4842.84	100008.52
P6$_t$	2.02	−5.05	−3.03	655	−5.73	−5.67	0.0043	1.82	3.26	3019.09	3829.10	82909.47

the polymer chain in solid-state. There are slight differences in the polymers' electronical and optical bandgaps, with Eg^{ec} being higher than E_g^{op} (Table 2). This could be attributed to the formation of free ions during electrochemical characterization instead of a naturally excited state.[71]

Another important characteristic of conducting polymers is the electrochromicity of the resulting polymers, which affects their applicability in different fields such as electrochromic devices, displays, mirrors, windows, and sunglasses. Electrochromic performances of the polymers were provided in supporting information. Electrochromic contrast and switching studies were performed to determine the polymers' switching times and percent transmittance changes (optical contrast). While the optical contrast could be defined as the change in percent transmittance between the two extreme states (neutral and oxidized states), the switching time is between the colored and bleached states of the electrochromic material at a 95% contrast value. The electrochromic contrast and switching measurements were performed between the polymers' neutral and fully oxidized states (the two extreme states) with 5 s time intervals. The percentage transmittance vs time graphs and data were provided in supporting information.

2.5. Computational Results

The trend in bandgap increases observed among **P1$_t$** to **P3$_t$** or **P4$_t$** to **P6$_t$** in theoretical studies is consistent with the experimental results (**Table 3**). The small variations in bandgap provided by thiophene and selenophene bridges indicate that the structure of the bridge may not be the primary determining factor for E_g. Instead, the structural composition of the polymers and donor-acceptor types play more crucial roles compared to the effect of bridge unit. Still, this study showed that fine-tuning the energy levels and detailed band-gap engineering can be applied by controlling the bridge units. The difference between the experimental and computational results can be attributed to the limitations in chain length and the interchain interactions that cannot be fully accounted for in theoretical calculations. Additionally, it should be noted that the composition of the Pn and Pnt, where n = 1,2,3,4,5,6, were not perfectly identical due to computational capacity since it is impossible to reach an exact experimental ratio for a tetramer structure.

P1$_t$ and **P4$_t$** exhibit relatively lower VIP, AIP, and λ_{reorg} values with the smallest **M1** and **M3** compositions, which are desirable electronic properties for a successful donor-acceptor chain that exhibits enhanced charge mobility. Particularly, **P4** demonstrates higher charge mobility compared to its thiophene-containing counterparts due to the increased π orbital overlap of the larger orbitals of selenium atoms, resulting in a higher current density in photovoltaic device applications (measured at 11.44 mA/cm^2). In the light of this information, the experimentally measured photovoltaic performance of **P4** (a power conversion efficiency (PCE) of 6.26%, an open-circuit voltage (V_{OC}) of 0.80 V, a short-circuit current density (J_{SC}) of 11.44 mA cm^{-2}, and a fill factor (FF) of 68.81%) aligns with the theoretically calculated reorganization energy, indicating higher charge mobility.

Table 3 presents the calculated absorption λ_{max} (nm), which decreases in the following order: **P4$_t$ > P5$_t$ > P6$_t$ > P1$_t$ > P2$_t$ > P3$_t$**, correlating with the bandgap energy due to increased π delocalization. Selenophene-containing copolymers exhibit red-shifted absorption spectra, consistent with experimental absorption results in solution or thin-film states. The dipole moment of structures increases in the same order as the bandgap energy, attributed to the increasing size of the bridging units. Conversely, polarizability and anisotropic polarizability show a decreasing trend from **P1$_t$** to **P3$_t$** and **P4$_t$** to **P6$_t$**, respectively, due to the increasing ratio of **M1** and **M3**. First-order hyperpolarizability, defining the ease of induced dipole formation in the presence of an electric field, is higher for **P4$_t$-P6$_t$** as expected due to the heavier selenium atom effect. Hyperpolarizability is proportional to the reduction of bond length alternation through the polymer backbone, as demonstrated in our previous study, showcasing enhanced electron delocalization for **P2t** and **P5t** with a composition of (X:0.5 Y:0.5) branched with thiophene and selenophene, respectively.[72]

ESP surfaces indicate strong donor-acceptor behavior along the backbone, representing electron-rich parts in red and electron-deficient parts in blue for both copolymers, as demonstrated in **Figure 4**. The increasing trend of localized electron-rich parts from **P1** to **P3** and **P4** to **P6** can be explained by the rising ratio of TPD units in the polymer backbone. The backbone of the copolymers is more occupied by the HOMO orbital, and LUMOs are highly concentrated on BO and TPD units for all copolymers. While orbital diagrams and ESP maps effectively illustrate the distribution of electron acceptors and donors along the chains, these visual representations lack the sensitivity required to recognize the distinctions imparted by the thiophene and selenophene bridge structures.

Dihedral angles between BO and bridging units of **M1** and **M3** are depicted in **Figure 5**a,b. The average dihedral angle is found to be 8.15° for the thiophene-bridged copolymer and 9.09° for the selenophene-bridged copolymer, indicating a slightly higher

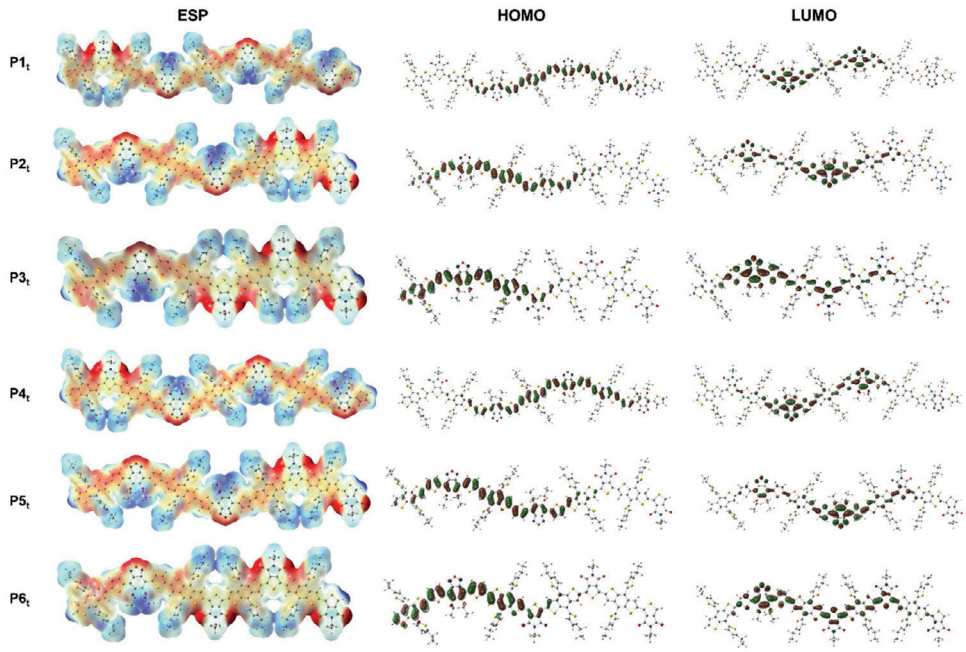

Figure 4. DFT-optimized ESP surface and frontier orbital distribution for **P1-P6**.

planarity achieved with the smaller atom-sized sulfur atom in the bridge unit.

Next, the TDDFT results were further utilized in the analysis and visualization of the atom-to-atom and inter-fragment charge transfer during $S_0 \rightarrow S_1$ excitation as heat maps (charge transfer matrix, CTM) to show the selenophene and thiophene bridging difference. TPD is attached to **M1** and **M3** units at both ends to exclude the end group effect. The CTMs were plotted to quantitatively analyze the inter-fragment charge transfer via the inter-fragment charge transfer (IFCT) method with the Multiwfn 3.6. The contributions of the electron-accepting part (fragment 1) and electron-rich part (fragment 2) of the molecules to holes and electrons for $S_0 \rightarrow S_1$ transitions are presented in **Table 4** and Figure 5c,d. For the selenophene bridge molecule, the electron on the acceptor part is increased by 0.368 during a single electron excitation, while the thiophene bridged acceptor part gains 0.389 electrons. CTMs in Figure 5e,f represent the atom-to-atom charge transfer, excluding the hydrogen, for thiophene and selenophene bridge monomers, respectively. Atom numbers 76 and 77 (S and Se-atom) in the thiophene or selenophene moiety transfer electrons to most atoms, representing a light blue color in the heat map of both bridged monomers.

2.6. Photovoltaic Studies

2.6.1. Device Fabrication

The bulk heterojunction organic solar cells were fabricated with a device structure of glass/ITO/PEDOT: PSS/active layer/LiF/Al. For the cleaning process, ITO-coated glass substrates were treated with an ultrasonic bath in Hellmanex, water, acetone, and isopropyl alcohol separately for 15 min, and oxygen plasma treatment was performed for 5 min. For hole transport layer PEDOT: PSS was filtered with PES 45 µm filter and coated onto the substrates with spin coater at 3500 rpm, followed by thermal annealing at 150 °C for 15 min. In the active layer, donor-acceptor type copolymers **P1**, **P2**, **P3**, **P4**, **P5**, and **P6** were used as donor

Table 4. Inter-fragment electron transfer analysis for $S_0 \rightarrow S_1$ excitation of thiophene- and selenophene-bridged BO in modeled monomeric units.

	Thiophene-bridge		Selenophene-bridge	
	Fragment 1	Fragment 2	Fragment 1	Fragment 2
Contribution to Hole	47.34%	52.66%	48.54%	51.46%
Contribution to Electron	86.25%	13.75%	85.37%	14.63%
Variation of population	0.389	-0.389	0.368	−0.368
Intra-fragment electron redistribution	0.408	0.072	0.414	0.075
Transferred electron between fragments	1→2: 0.065 1←2: 0.454 Net 1→2: – 0.389		1→2: 0.071 1←2: 0.439 Net 1→2: – 0.368	

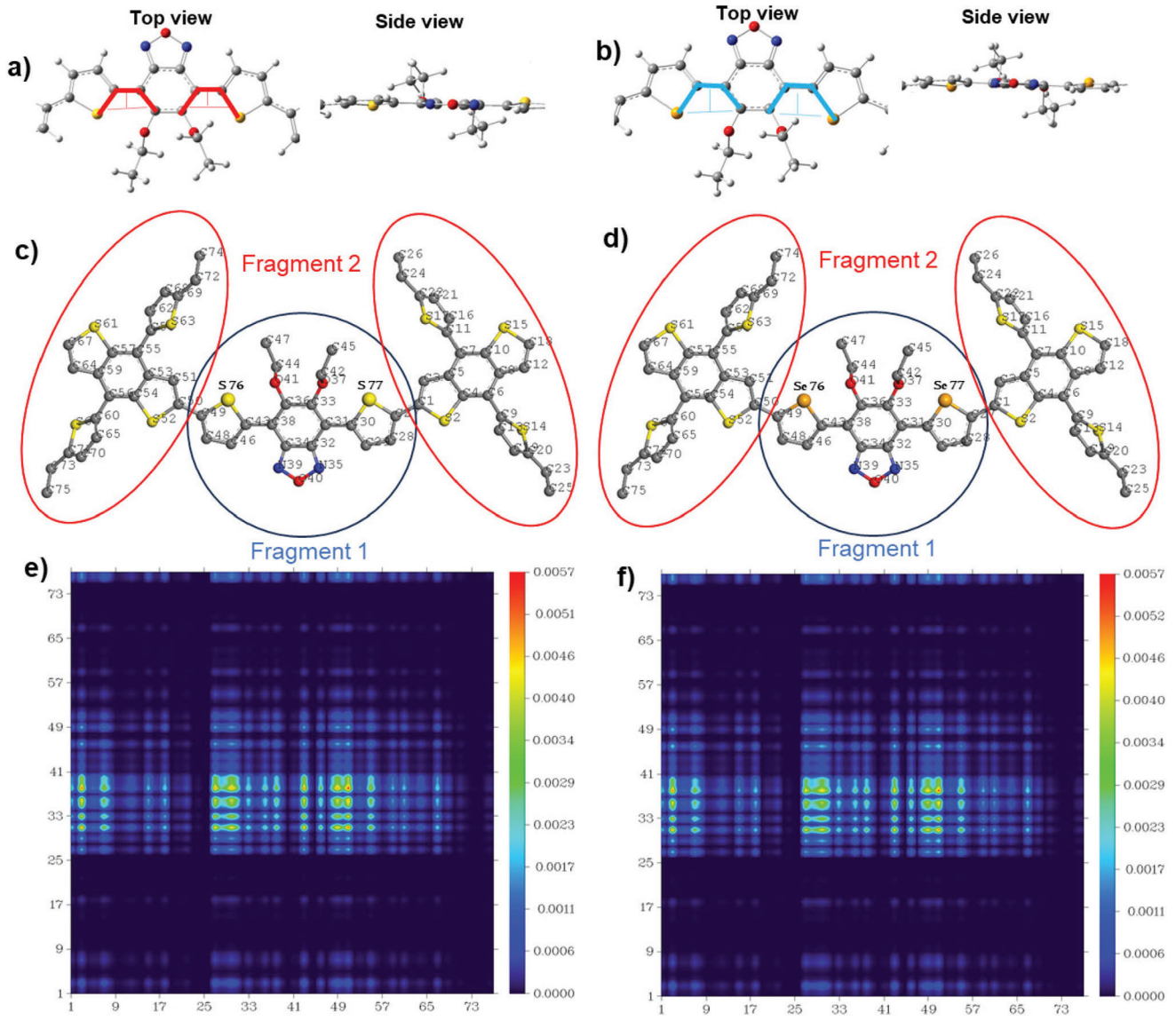

Figure 5. Top and side view of the optimized structure of a) $\mathbf{P1_t}$ and b) $\mathbf{P4_t}$. Red and blue dashed lines represent the corresponding dihedral angles. Numbering of atoms and fragments in c) thiophene and d) selenophene bridged monomers. Heat maps of the atom-to-atom charge transfer matrix for S1 ← S0 excitation of e) thiophene and d) selenophene bridged monomers.

Table 5. The photovoltaic performances and device parameters of champion devices.

Polymer: $PC_{71}BM$ Ratio	Spin Coating (rpm)	Conc. (%)	Additive	V_{OC} (V)	J_{sc} (mA cm^{-2})	FF (%)	PCE (%)
P1 (1:3)	750	2.0	9% DPE	0.88	6.90	57.97	**3.59**
P2 (1:3)	750	2.0	–	0.90	6.03	55.80	**3.12**
P3 (1:3)	500	2.0	–	0.94	6.74	54.40	**3.67**
P4 (1:2)	750	2.5	6% DPE	0.80	11.44	68.81	**6.26**
P5 (1:3)	750	2.0	–	0.85	8.78	53.67	**4.02**
P6 (1:3)	750	2.0	3% DPE	0.86	7.04	60.02	**3.65**

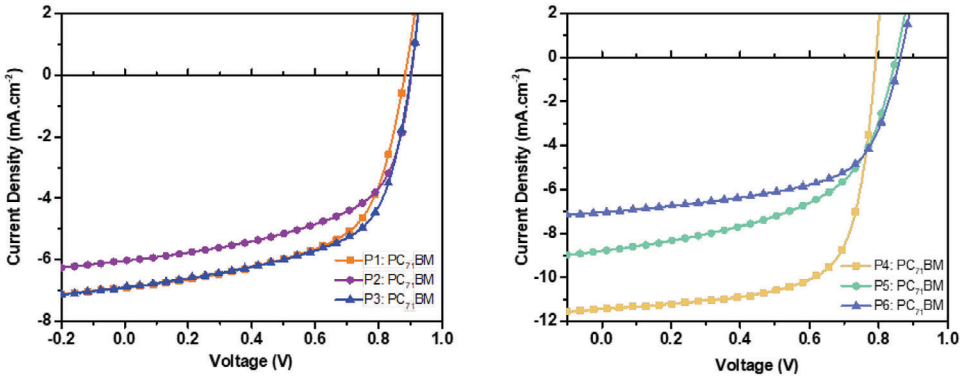

Figure 6. *J–V* curves of P1-P3: $PC_{71}BM$ (left) and P4-P6: $PC_{71}BM$ (right) constituted OSCs.

material and blended with fullerene acceptor $PC_{71}BM$, then coated onto hole transport layer with spin coater inside a glove box system under N_2 atmosphere. These active layer coated substrates were annealed at 110 °C for 10 min, then LiF and Al were deposited onto the active layer in 0.6 and 100 nm thickness, respectively, via a metal evaporator under vacuum conditions (10^{-7} Torr). Optimizations were carried out by solvent selection, changing the weight percentage of the blend, donor polymer: $PC_{71}BM$ weight ratio, and thickness of the active layer to obtain the best results. Also, DIO and DPE additives were used in the active layer to improve morphology.

2.6.2. Photovoltaic Performance

Organic solar cell devices were fabricated using conventional device architecture of ITO/PEDOT: PSS/active layer/LiF/Al. Donor-π -acceptor type copolymers **P1**, **P2**, **P3**, **P4**, **P5**, and **P6** were used as donors and $PC_{71}BM$ as acceptors in the active layer of the solar cell to investigate the effect of utilizing selenophene and thiophene as an π bridge and the ratio of acceptor moieties in the copolymer compositions. Copolymers **P1-P3** consist of thiophene as a π bridge, while selenophene is used in copolymers **P4-P6**. Also, the ratio of acceptor monomer in copolymers varies to 80:20, 60:40, and 40:60 (BO: TDP), respectively. $PC_{71}BM$ was preferred as an acceptor due to its broad absorption compared to $PC_{61}BM$.[73] To obtain the best results for each polymer optimization process, which involves changing the thickness of the active layer, donor: $PC_{71}BM$ w/w ratio, the concentration of the active layer, and the selection of the proper solvent were carried out. The thickness of the active layer is altered through various coating speeds, starting from 500 rpm and going up to 1500 rpm. The best results were obtained from 500 rpm for **P3** and 750 rpm for **P1**, **P2**, **P4**, **P5**, and **P6**. Active layer thicknesses of 101, 97, 106, 135, 111, and 117 nm were obtained for **P1**, **P2**, **P4**, **P5**, and **P6**, respectively. Donor: $PC_{71}BM$ wt ratio of active layer blend was varied as 1:1, 1:2, 1:3, and 1:4 throughout the experiments. The optimum weight ratio was 1:3 for almost all six polymers except **P4**, which works best with a 1:2 Donor: $PC_{71}BM$ wt ratio. OSC devices with 2% active layer concentration improved performance for **P1**, **P2**, **P3**, and **P5**, while active layers with 2.5% and 3% concentration worked best for **P4** and **P6**, respectively. Chlorobenzene, ortho-dichlorobenzene, and chloroform were used as sol-

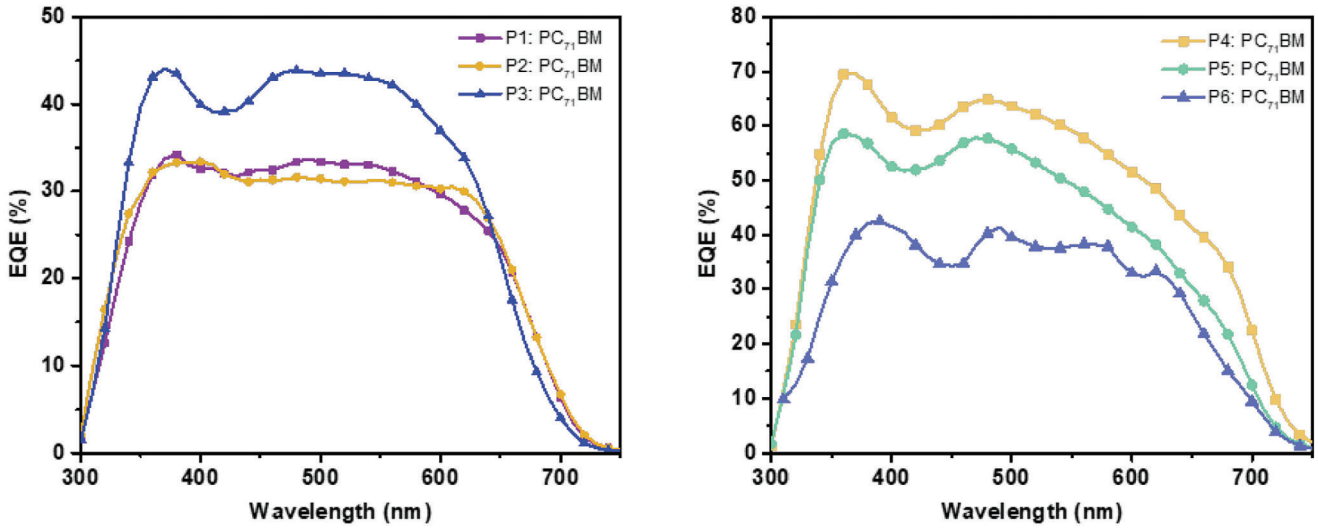

Figure 7. EQE curves of **P1-P3**: $PC_{71}BM$ (left) and **P4-P6**: $PC_{71}BM$ (right) constituted OSCs.

vents in the donor-acceptor blend to determine the appropriate solvent showing the best results. Ortho-dichlorobenzene was selected as the optimum solvent for **P2**, **P3**, **P4**, **P5**, and **P6**. Meanwhile, devices with chlorobenzene showed better performance for copolymer **P1**.

The photovoltaic performances of the best devices for all six polymers are summarized in **Table 5**, and the best results were obtained from copolymer **P4**, which contains selenophene as π-bridge among all six polymers with a PCE of **6.26%,** a V_{OC} of 0.80 V, a J_{SC} of 11.44 mA cm^{-2} and FF of 68.81%. Adding 6% DPE improved the PCE from 5.04% to 6.26% and J_{SC} from 9.36 to 11.44 mA cm^{-2} by providing better morphology. Additionally, among three thiophene-bridged copolymers (**P1-P3**), the highest device performance was observed in the copolymer **P3**, where the acceptor ratio in the copolymer is 40:60. **P3**-based OSC device's photovoltaic performance improved by the addition of 2% DIO since PCE and FF values were advanced from 3.67% and 54.46% to 3.73% and 57.83%, respectively, while DPE addition reduced the device performance.

In **P1**-based OSCs, changing the donor: $PC_{71}BM$ weight ratio from 1:2 to 1:3 increased the PCE value from 2.35% to 3.59% and V_{OC} from 0.86 to 0.89 V. Also, adding 9% DPE provided the best photovoltaic performance, while devices with 1% and 2% DIO additives gave poor results and did not properly function. OSCs based on **P2** showed a PCE of 3.12%, a V_{OC} of 0.90 V, a J_{SC} of 6.03 mA cm^{-2}, and an FF of 55.80%. The photovoltaic performance of devices did not improve with the addition of either DPE or DIO. In OSCs based on **P5**, altering the donor-acceptor wt ratio had a significant impact on photovoltaic performance since PCE and J_{SC} values increased from 2.42% and 5.19 mA cm^2 to 4.02 and 8.78 mA cm^2, respectively, as the donor: $PC_{71}BM$ ratio changed from 1:2 (w/w) to 1:3 (w/w). **P6**-based OSCs' device performance was enhanced through 3% DPE addition due to its improved PCE and J_{SC} values from 2.63% and 6.17% to 3.65% and 7.04 mA cm^{-2}, whereas DIO decreases the photovoltaic performance.

A remarkable trend could be observed from Table 5, when the V_{OC} values of the OSCs were considered, there was an increment in the V_{OC} values from **P1** to **P3** and **P4** to **P6** as TPD moiety increased in the copolymer. Since the V_{OC} value of organic solar cells strongly depends on the HOMO level of the donor polymer,[74] the enhanced V_{OC} values can be attributed to the TPD structure due to its strong electron-accepting nature leading low lying HOMO levels.[75–77] Conversely, as the ratio of BO unit with the π-bridges ratio of the copolymer decreases, the J_{SC} values of OSCs were mostly reduced. This trend could be explained by the better absorption ability of the BO structure with the π-bridges, which may have a great influence on the short-circuit current values of the OSC devices.[69] In **Figure 6**, the *J*–*V* curves of the devices are shown.

When device performances of D- π -A_1- π – D – A_2 – D type copolymers, which have the same ratio, are compared, the effect of utilizing selenophene or thiophene as π bridge can be observed clearly. Selenophene π bridge in copolymer **P4** enhanced the photovoltaic performance compared to thiophene in copolymer **P1** since the PCE increased from 3.59% to 6.26%. A similar trend was also seen in **P2** and **P5**, where the PCE value increased from 3.12% to 4.02%. The rationale behind the advanced photovoltaic performance of selenophene-based copolymers can be explained by the intermolecular Se-Se interactions leading to better intermolecular charge mobility and π orbital overlap of the larger orbitals of Selenium atoms, which facilitates better conductivity and charge mobility.[70,78,79] Additionally, the PCE value of **P3**-based OSC was slightly higher than **P6**-based devices. Since the π bridge part ratio is less in the copolymer, the influence of π bridge on photovoltaic performance might be suppressed by TPD containing part of the copolymer. Moreover, Selenophene and thiophene π bridges do not have a significant impact on HOMO-LUMO levels of the copolymers since there is no meaningful difference between HOMO-LUMO levels of **P1** and **P4**, which have the highest π bridge component among **P1-P6**. In **Figure 7**, the external quantum efficiencies (EQE) of the best devices were represented.

Between the 300–750 nm wavelength range, all the active layer materials (Polymer: PCBM) showed a response that is consistent with the absorption of the polymers. The maximum EQE values are 44%, 34%, and 33% for **P1**, **P3**, and **P2**, respectively. For **P4**, **P5**, and **P6**, EQEs were found as 70%, 59%, and 42%, respectively. The J_{SC} values that are acquired from the *J*–*V* curves are consistent with the values that are obtained from the EQE curves.

2.6.3. Morphology

Morphological and topographical analyses were performed using atomic force microscopy (AFM) and transmission electron microscopy (TEM). **Figure 8** illustrates the height images of the best devices with **P1-P6** blends. The root mean square roughness (Rq) values for **P1**, **P2**, and **P3** blends were measured as 1.06, 1.77, and 2.23 nm, respectively, indicating comparable surface roughness. In addition, RMS roughness values for the best devices of **P4**, **P5**, and **P6** blends were 1.22, 5.40, and 0.97 nm, respectively. A substantial rise in roughness values from 1.22 to 5.40 nm can be responsible for the dramatic decrease in FF values from 68.81% to 53.67% when **P4** and **P5** blends are compared. Also, the roughness value for **P6** was relatively low compared to the other six polymer blends, which indicates a smoother surface consistent with its high FF value.[80] Although **P6** seemed to have better morphology than **P4** and **P5** blends, its *J*sc value, therefore its PCE value, was the lowest due to its poor light absorption. Also, when the roughness of **P1** and **P4** blends were compared to observe the impact of the Selenophene and Thiophene π bridge on morphology, there was no significant morphological difference since the Rq values were quite similar.

TEM images of the **P1-P6** blends are displayed in **Figure 9**. Figure 9A–C,F correspond to the TEM views of **P1**, **P2**, **P3**, and **P6** blends, which involve large $PC_{71}BM$ and polymer domains, leading to no bicontinuity through active layer surface, thus poor photovoltaic performance parameters obtained in terms of FF and J_{SC}.[81] Figure 9D,E illustrate the TEM views of the **P4** and **P5** blends exhibiting bicontinuous donor and acceptor domains. Thus, the higher photovoltaic performance of the **P4** and **P5** can be attributed to a more homogenous donor-acceptor blend on the active layer surface, leading to better exciton diffusion and dissociation.[78,82,83]

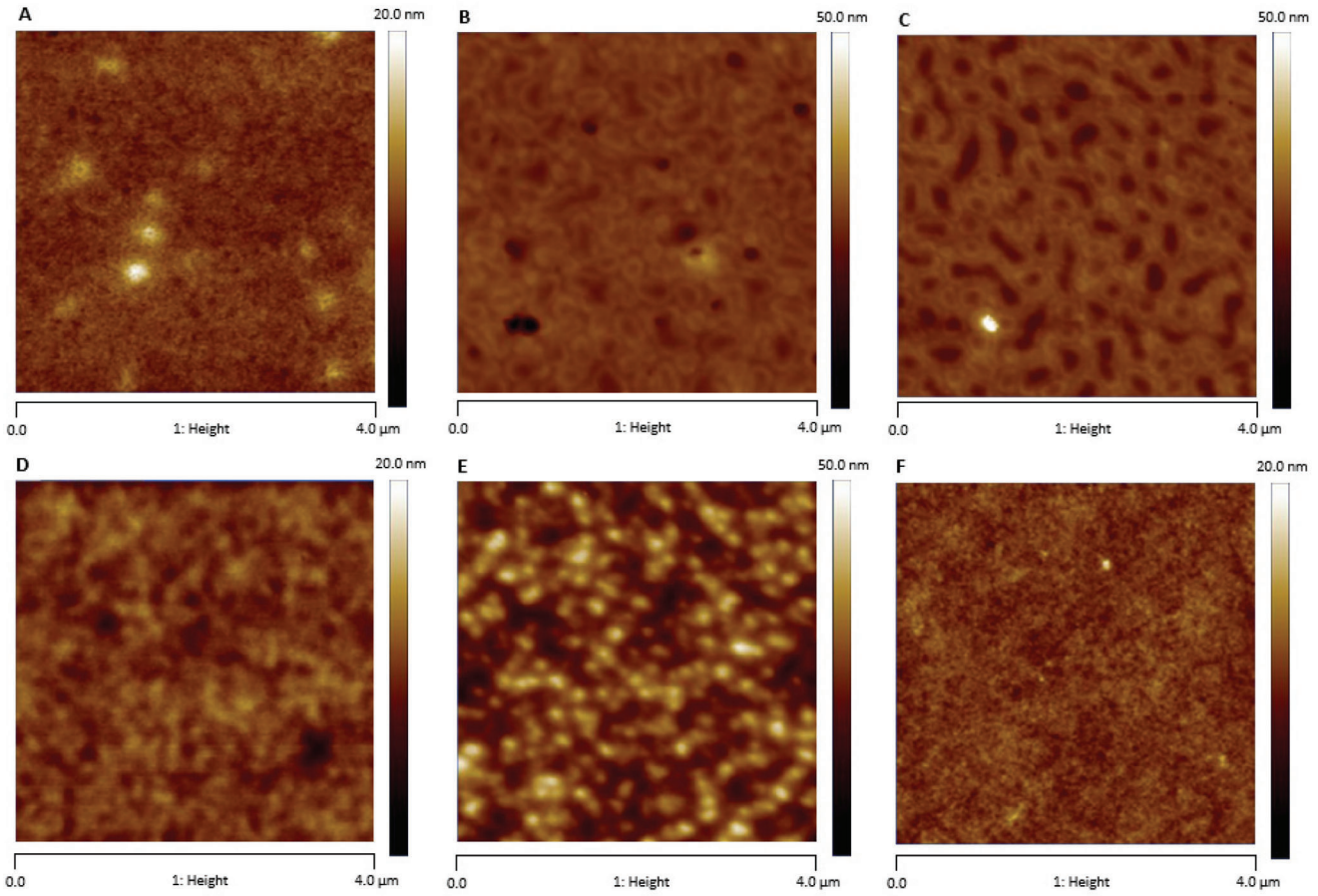

Figure 8. AFM images of A) P1:$PC_{71}BM$ (1:3, 9% DPE), B) P2:$PC_{71}BM$ (1:3), C) P3:$PC_{71}BM$ (1:3), D) P4:$PC_{71}BM$ (1:2, 6% DPE), E) P5:$PC_{71}BM$ (1:3), F) P6:$PC_{71}BM$ (1:3, 3% DPE).

3. Conclusion

In this study, six different novel donor-π-acceptor$_1$-π-donor-acceptor$_2$ type random co-polymer structures were prepared by using thiophene and selenophene bridges in polymer structures containing BDT as donor and BO and TPD as acceptors. The impact of the π-bridge and acceptor core ratios was thoroughly studied in terms of optical, electrochemical, and photovoltaic functionality in these designs. To investigate how the acceptor unit ratio and replacement of aromatic bridge units impact the structural, electronic, and optical properties of the polymers, density functional theory (DFT) calculations were carried out for the tetramer models. The results of optical and electronical studies are consistent with the theoretical findings. All the polymers showed good thermal stability with higher T_d than 310 °C. The properties of **P1-P3** and **P4-P6** changed as the π-bridge was chosen as thiophene and selenophene, respectively. The bandgaps of the **P1** and **P4** were tuned from 1.70 to 1.67 eV, with HOMO levels decreasing from −5.52 to −5.61 eV. The maximum absorption wavelengths λ_{max} were shifted from 587/633 to 606/650 nm, respectively. Our study showed that the open-circuit voltage (V_{OC}), which is strongly correlated with the HOMO levels of the donor material, was enhanced with the increasing ratio of the TPD moiety in the polymer due to its strong electron-accepting nature leading low lying HOMO levels. On the other hand, the short-circuit current (J_{SC}), which is associated with the absorption ability of the donor material, was improved by the increasing ratio of BO moiety with the π-bridges. Due to their well-established morphology and charge transport properties, the PCBM/P3HT systems are well-known for their balanced performance with moderate efficiencies, typically ≈3%–5%. However, our selenophene-bridged copolymer, particularly **P4**, achieved a power conversion efficiency (PCE) of 6.26%, significantly surpassing typical PCBM/P3HT systems. Additionally, the incorporation of selenophene bridges and TPD cores has resulted in more efficient charge separation and transport, as evidenced by the higher J_{SC} and V_{OC} values obtained. Jiang et al. (2014) thoroughly examined the photovoltaic properties of a polymer structure consisting of BO, BDT, and a thiophene bridge and reported a PCE value of **5.9%**.[68] This study presents the highest PCE value of **6.29%** with a short-circuit density (J_{SC}) of 11.44 mA cm^{-2}, an open-circuit voltage (V_{OC}) of 0.80 V, and a fill factor (FF) of 68.81%, which was achieved with applying a modification on polymer backbone by incorporating a selenophene bridge and TPD core distinctly from its literature analog. As a result, enhanced performance of the constructed solar device is achieved by improved morphology and better absorption ability.

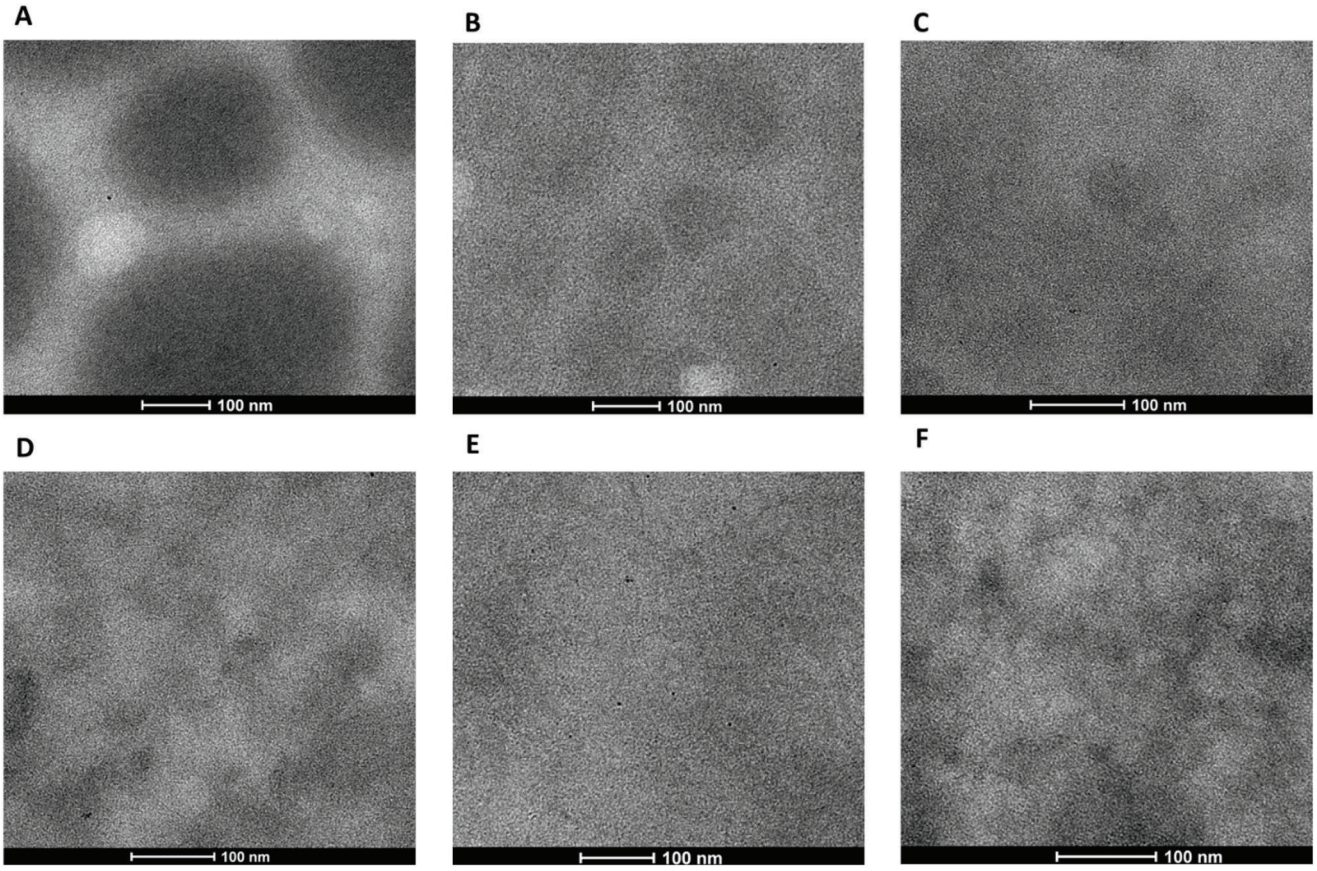

Figure 9. TEM images of A) P1:$PC_{71}BM$ (1:3, 9% DPE), B) P2:$PC_{71}BM$ (1:3), C) P3:$PC_{71}BM$ (1:3), D) P4:$PC_{71}BM$ (1:2, 6% DPE), E) P5:$PC_{71}BM$ (1:3), F) P6:$PC_{71}BM$ (1:3, 3% DPE). The scale bar is 100 nm.

Supporting Information

Supporting Information is available from the Wiley Online Library or from the author.

Received: May 13, 2024
Revised: July 4, 2024
Published online:

Acknowledgements

Oğuzhan Karakurt and Levent Kamil Toppare were thankful for financial support from the Scientific and Technological Research Council of TURKEY (TUBITAK) with project number 121C274. The numerical calculations reported in this paper were partially performed at TUBITAK ULAKBIM, High Performance and Grid Computing Center (TRUBA resources) and National Center for High Performance Computing of Turkey (UHeM).

Conflict of Interest

The authors declare no conflict of interest.

Data Availability Statement

The data that support the findings of this study are available in the supplementary material of this article.

Keywords

Benzoxadiazole, density functional theory, donor–acceptor copolymers, organic photovoltaics, thienopyrrole

[1] G. Li, R. Zhu, Y. Yang, *Nat. Photonics* **2012**, *6*, 153.
[2] W. Yue, X. Huang, J. Yuan, W. Ma, F. C. Krebs, D. Yu, *J. Mater. Chem. A* **2013**, *1*, 10116.
[3] T. L. Nguyen, H. Choi, S.-J. Ko, M. A. Uddin, B. Walker, S. Yum, J.-E. Jeong, M. H. Yun, T. J. Shin, S. Hwang, J. Y. Kim, H. Y. Woo, *Energy Environ. Sci.* **2014**, *7*, 3040.
[4] Q. Tao, Y. Xia, X. Xu, S. Hedström, O. Bäcke, D. I. James, P. Persson, E. Olsson, O. Inganäs, L. Hou, W. Zhu, E. Wang, *Macromolecules* **2015**, *48*, 1009.
[5] O. Karakurt, E. Alemdar, M. C. Erer, D. Cevher, S. Gulmez, U. Taylan, S. C. Cevher, G. Hizalan Ozsoy, B. Ortac, A. Cirpan, *Dyes Pigm.* **2022**, *208*, 110818.
[6] D. Gedefaw, M. Tessarolo, M. Bolognesi, M. Prosa, R. Kroon, W. Zhuang, P. Henriksson, K. Bini, E. Wang, M. Muccini, M. Seri, M. R. Andersson, *Beilstein J. Org. Chem.* **2016**, *12*, 1629.
[7] J.-H. Kim, H. U. Kim, C. E. Song, I.-N. Kang, J.-K. Lee, W. S. Shin, D.-H. Hwang, *Sol. Energy Mater. Sol. Cells* **2013**, *108*, 113.
[8] T. J. Kim, T. D. Kim, *Mol. Cryst. Liq. Cryst.* **2017**, *644*, 124.
[9] L. Qin, X. Li, C. Dong, J. Zhou, Q. Guo, A. Tang, Y. Zhong, E. Zhou, *Chem. Eng. J.* **2023**, *464*, 142743.

[10] Z. He, T. Dai, M. Ji, A. Tang, H. Wang, E. Zhou, *ACS Macro Lett.* **2023**, *12*, 1144.
[11] X. Li, A. Tang, H. Wang, Z. Wang, M. Du, Q. Guo, Q. Guo, E. Zhou, *Angew. Chem. – Int. Ed.* **2023**, *62*, e202306847.
[12] V. Tamilavan, D. Kim, H.-S. Yang, I. Shin, J. Kim, B. R. Lee, S. H. Park, *Macromol. Chem. Phys.* **2022**, *223*, 2200222.
[13] S. Al-Isaee, A. Iraqi, D. Lidzey, *Tetrahedron* **2023**, *138*, 133416.
[14] C. Z. Karaman, S. Göker, Ü. Şahin, S. O. Hacioglu, S. T. Aslan, T. Hacıefendioğlu, G. Hizalan, E. Yıldırım, A. Çırpan, L. Toppare, *J. Electroanal. Chem.* **2021**, *895*, 115483.
[15] M. Iqbal, A. Hussain, A. Naz, R. Hussain, M. Yar, K. Ayub, M. R. H. Shah Gilani, M. Imran, M. A. Assiri, *Spectrochim. Acta – A: Mol. Biomol. Spectrosc.* **2023**, *291*, 122322.
[16] X. Hu, R. Datt, Q. He, P. Kafourou, H. Ka Hin Lee, A. J. P. White, W. C. Tsoi, M. Heeney, *J. Mater. Chem. C* **2022**, *10*, 9249.
[17] Y. He, Q. Wang, X. Jing, Y. Zhao, C. Gao, X. Zhai, X. Wang, L. Yu, M. Sun, *Org. Electron.* **2022**, *101*, 106424.
[18] S. T. Aslan, D. Cevher, E. Bolayır, G. Hizalan Ozsoy, Y. Arslan Udum, E. Yıldırım, L. Toppare, A. Cirpan, *Electrochim. Acta* **2021**, *398*, 139298.
[19] Y. Song, Z. Zhong, L. Li, X. Liu, J. Huang, H. Wu, M. Li, Z. Lu, J. Yu, J. Hai, *Chem. Eng. J.* **2022**, *430*, 132830.
[20] M. Pu, X. Lai, H. Chen, C. Cao, Z. Wei, Y. Zhu, L. Tian, F. He, *J. Energy Chem.* **2023**, 19.
[21] S. A. Shin, J.-H. Kim, J. B. Park, I.-N. Kang, M.-J. Park, D.-H. Hwang, *Macromol. Chem. Phys.* **2013**, *214*, 1780.
[22] J.-H. Kim, S. A. Shin, J. B. Park, C. E. Song, W. S. Shin, H. Yang, Y. Li, D.-H. Hwang, *Macromolecules* **2014**, *47*, 1613.
[23] H. M. Ng, C. H. Kwok, Z. Qi, Z. Wang, L. Chen, W. Liu, W. Zhao, H. Ade, C. Zhang, H. Yan, H. Yu, *J. Mater. Chem. A* **2023**, *11*, 22769.
[24] S. Kutkan, S. Goker, S. O. Hacioglu, L. Toppare, *J. Macromol. Sci., Part A: Pure Appl. Chem.* **2016**, *53*, 475.
[25] L. Zeng, R. Ma, Q. Zhang, T. Liu, Y. Xiao, K. Zhang, S. Cui, W. Zhu, X. Lu, H. Yan, Y. Liu, *Mater. Chem. Front.* **2021**, *5*, 1906.
[26] H. You, H. Kang, D. Kim, J. S. Park, J.-W. Lee, S. Lee, F. S. Kim, B. J. Kim, *ChemSusChem* **2021**, *14*, 3520.
[27] C. Zhu, L. Meng, J. Zhang, S. Qin, W. Lai, B. Qiu, J. Yuan, Y. Wan, W. Huang, Y. Li, *Adv. Mater.* **2021**, *33*, 2100474.
[28] B. Sun, Y. Chen, Y. Huang, Y. Li, J. Fan, *Org. Electron.* **2021**, *98*, 106282.
[29] S. W. Lee, M. W. Hussain, S. Shome, S. R. Ha, J. T. Oh, D. R. Whang, Y. Kim, D.-Y. Kim, H. Choi, D. W. Chang, *Sci. Rep.* **2021**, *11*, 24381.
[30] M. R. Busireddy, T.-W. Chen, S.-C. Huang, H. Nie, Y.-J. Su, C.-T. Chuang, P.-J. Kuo, J.-T. Chen, C.-S. Hsu, *ACS Appl. Mater. Interfaces* **2022**, *14*, 22353.
[31] E. H. Jung, H. Ahn, W. H. Jo, J. W. Jo, J. W. Jung, *Dyes Pigm.* **2019**, *161*, 113.
[32] M. Shaker, M. M. El-Hendawy, B. Park, K. Lee, *New J. Chem.* **2019**, *43*, 18126.
[33] B. Shahid, D. Zhu, Q. Wang, X. Yuan, I. Ismail, Y. Wu, Z. Du, R. Yang, *Polym. Int.* **2020**, *69*, 564.
[34] M. M. Tepliakova, I. E. Kuznetsov, I. A. Avilova, K. J. Stevenson, A. V. Akkuratov, *Macromol. Chem. Phys.* **2021**, *222*, 2170029.
[35] W. Guo, H. Liu, J. Liu, J. Zhang, Y. Cao, Z. Yang, Y. Liu, Z. Wu, X. Song, Y. Niu, Y. Liu, *Synth. Met.* **2021**, *277*, 116768.
[36] Z. Li, C. Liu, J. Liu, C. Long, Y. Chen, X. Huang, L. Wei, N. Qiu, *New J. Chem.* **2023**, *47*, 17406.
[37] T. N.-L. Phan, J.-W. Lee, E. S. Oh, S. Lee, C. Lee, T.-S. Kim, S. Li, B. J. Kim, *ACS Appl. Mater. Interfaces* **2022**, *14*, 57070.
[38] J. Wu, S. Yang, S. Wang, Z. Jiang, C. Gao, L. Wang, *Compos. Commun.* **2023**, *37*, 101461.
[39] X. Lin, S. Tu, L. Xiao, H. Zhen, W. Wang, Q. Ling, *Chem. Eng. J.* **2023**, *464*, 142634.
[40] M. H. Maqsood, R. A. Khera, R. F. Mehmood, S. J. Akram, N. Al-Zaqri, M. A. A. Ibrahim, S. Noor, M. Waqas, *J. Mol. Grap. Model.* **2023**, *124*, 108550.
[41] S. Taskaya Aslan, E. Alemdar Yılmaz, T. Hacıefendioğlu, Y. Arslan Udum, L. Toppare, E. Yıldırım, A. Cirpan, *Eur. Polym. J.* **2022**, *169*, 111141.
[42] M. L. Keshtov, I. O. Konstantinov, D. Y. Godovsky, I. E. Ostapov, V. G. Alekseev, A. Agrawal, H. Dahiya, G. D. Sharma, *Energy Technol.* **2022**, *10*, 2200215.
[43] V. S. Kadam, H. K. Machhi, S. S. Soni, S. S. Zade, A. L. Patel, *New J. Chem.* **2022**, *46*, 8601.
[44] D. T. Le, N. T. T. Truong, T. H. Luu, L.-T. T. Nguyen, M. H. Hoang, H. P. K. Huynh, S. T. Cu, Q. T. Nguyen, H. T. Nguyen, *J. Polym. Res.* **2022**, *29*, 111.
[45] M. Yasa, L. Toppare, *Macromol. Chem. Phys.* **2022**, *223*, 2100421.
[46] B. Li, Q. Zhang, G. Dai, H. Fan, X. Yuan, Y. Xu, B. Cohen-Kleinstein, J. Yuan, W. Ma, *J. Mater. Chem. C* **2019**, *7*, 12641.
[47] C.-Y. Liao, Y. Chen, C.-C. Lee, G. Wang, N.-W. Teng, C.-H. Lee, W.-L. Li, Y.-K. Chen, C.-H. Li, H.-L. Ho, P. H.-S. Tan, B. Wang, Y.-C. Huang, R. M. Young, M. R. Wasielewski, T. J. Marks, Y.-M. Chang, A. Facchetti, *Joule* **2020**, *4*, 189.
[48] B. Zhao, H. Wu, W. Wang, H. Liu, J. Liu, Z. Cong, C. Gao, *React. Funct. Polym.* **2019**, *145*, 104378.
[49] V. Tamilavan, J. Lee, R. Agneeswari, D. Y. Lee, S. Cho, Y. Jin, S. H. Park, M. H. Hyun, *Polymer* **2015**, *65*, 243.
[50] L. Hu, J. Han, W. Qiao, Z. Y. Wang, *Polymer* **2016**, *99*, 427.
[51] M. Lu, W. Wang, W. Lv, S. Yan, T. Zhang, H. Zhen, Q. Ling, *RSC Adv.* **2016**, *6*, 86276.
[52] B. A. Alqurashy, *ChemistryOpen* **2019**, *8*, 429.
[53] S. Song, S.-J. Ko, H. Shin, Y. Jin, I. Kim, J. Young Kim, H. Suh, *Sol. Energy Mater. Sol. Cells* **2013**, *112*, 120.
[54] S.-M. Bang, J.-H. Park, S. Kang, Y.-S. Lee, B. Lim, H. Heo, J. Lee, Y. Lee, S.-I. Na, *Dyes Pigm.* **2017**, *140*, 229.
[55] M. Caliskan, M. C. Erer, S. T. Aslan, Y. A. Udum, L. Toppare, A. Cirpan, *Dyes Pigm.* **2020**, *180*, 108479.
[56] P. Sista, M. C. Biewer, M. C. Stefan, *Macromol. Rapid Commun.* **2012**, *33*, 9.
[57] E. Zhu, G. Ge, J. Shu, M. Yi, L. Bian, J. Hai, J. Yu, Y. Liu, J. Zhou, W. Tang, *J. Mater. Chem. A* **2014**, *2*, 13580.
[58] B. Liu, X. Chen, Y. He, Y. Li, X. Xu, L. Xiao, L. Li, Y. Zou, *J. Mater. Chem. A* **2013**, *1*, 570.
[59] L. Bian, E. Zhu, J. Tang, W. Tang, F. Zhang, *Prog. Polym. Sci.* **2012**, *37*, 1292.
[60] S. Goker, G. Hizalan, S. Kutkan, Y. Arslan Udum, A. Cirpan, L. Toppare, *J. Polym. Sci., Part A: Polym. Chem.* **2016**, *54*, 2459.
[61] P. Ding, C. Zhong, Y. Zou, C. Pan, H. Wu, Y. Cao, *J. Phys. Chem. C* **2011**, *115*, 16211.
[62] E. A. Yilmaz, M. Yasa, A. Cirpan, L. Toppare, *J. Electroanal. Chem.* **2023**, *932*, 117213.
[63] W. Jang, H. Cheon, S. Park, J. S. Cho, M. Yi, S.-K. Kwon, Y.-H. Kim, D. H. Wang, *Dyes Pigm.* **2017**, *145*, 29.
[64] X. Wang, Y. Sun, S. Chen, X. Guo, M. Zhang, X. Li, Y. Li, H. Wang, *Macromolecules* **2012**, *45*, 1208.
[65] J.-M. Jiang, P.-A. Yang, H.-C. Chen, K.-H. Wei, *Chem. Commun.* **2011**, *47*, 8877.
[66] D. J. Crouch, P. J. Skabara, J. E. Lohr, J. J. W. McDouall, M. Heeney, I. McCulloch, D. Sparrowe, M. Shkunov, S. J. Coles, P. N. Horton, M. B. Hursthouse, *Chem. Mater.* **2005**, 6567.
[67] W.-H. Chang, L. Meng, L. Dou, J. You, C.-C. Chen, Y. (.M.). Yang, E. P. Young, G. Li, Y. Yang, *Macromolecules* **2015**, *48*, 562.
[68] J.-M. Jiang, P. Raghunath, H.-K. Lin, Y.-C. Lin, M. C. Lin, K.-H. Wei, *Macromolecules* **2014**, *47*, 7070.
[69] J.-M. Jiang, H.-C. Chen, H.-K. Lin, C.-M. Yu, S.-C. Lan, C.-M. Liu, K.-H. Wei, *Polym. Chem.* **2013**, *4*, 5321.

[70] H.-Y. Chen, S.-C. Yeh, C.-T. Chen, C.-T. Chen, *J. Mater. Chem.* **2012**, *22*, 21549.
[71] D. Baran, A. Balan, S. Celebi, B. Meana Esteban, H. Neugebauer, N. S. Sariciftci, L. Toppare, *Chem. Mater.* **2010**, *22*, 2978.
[72] T. Haclefendioğlu, E. Yildirim, *ACS Omega* **2022**, 38969.
[73] F. Zhang, Z. Zhuo, J. Zhang, X. Wang, X. Xu, Z. Wang, Y. Xin, J. Wang, J. Wang, W. Tang, Z. Xu, Y. Wang, *Sol. Energy Mater. Sol. Cells* **2012**, 71.
[74] M. C. Scharber, D. Mühlbacher, M. Koppe, P. Denk, C. Waldauf, A. J. Heeger, C. J. Brabec, *Adv. Mater.* **2006**, *18*, 789.
[75] C. Garcias-Morales, D. Romero-Borja, J.-L. Maldonado, A. Roa, M. Rodríguez, J. García-Merinos, A. Ariza-Castolo, *Molecules* **2017**, *22*, 1607.
[76] Y. S. Choi, T. J. Shin, W. H. Jo, *ACS Appl. Mater. Interfaces* **2014**, *6*, 20035.
[77] K. Wang, Z. Xu, B. Guo, X. Guo, M. Zhang, Y. Li, *RSC Adv.* **2016**, *6*, 63338.
[78] N. Chakravarthi, K. Kranthiraja, M. Song, K. Gunasekar, P. Jeong, S.-J. Moon, W. Suk Shin, I.-N. Kang, J. W. Lee, S.-H. Jin, *Sol. Energy Mater. Sol. Cells* **2014**, *122*, 136.
[79] T. Xu, J. Lv, K. Yang, Y. He, Q. Yang, H. Chen, Q. Chen, Z. Liao, Z. Kan, T. Duan, K. Sun, J. Ouyang, S. Lu, *Energy Environ Sci* **2021**, *14*, 5366.
[80] S.-H. Lee, D.-H. Kim, J.-H. Kim, G.-S. Lee, J.-G. Park, *J. Phys. Chem. C* **2009**, *113*, 21915.
[81] K. Gao, Y. Kan, X. Chen, F. Liu, B. Kan, L. Nian, X. Wan, Y. Chen, X. Peng, T. P. Russell, Y. Cao, A. K.-Y. Jen, *Adv. Mater.* **2020**, *32*, 1906129.
[82] L. Zhu, M. Zhang, J. Xu, C. Li, J. Yan, G. Zhou, W. Zhong, T. Hao, J. Song, X. Xue, Z. Zhou, R. Zeng, H. Zhu, C.-C. Chen, R. C. I. MacKenzie, Y. Zou, J. Nelson, Y. Zhang, Y. Sun, F. Liu, *Nat. Mater.* **2022**, *21*, 656.
[83] X. Zhu, L. Yang, Y. Pan, Y. Yang, X. Ding, C. Wan, Z. Zhang, Y. Luo, Q. Zhou, L. Wang, S. Xiao, *Chemistry* **2024**, *30*, e202304167.

